A Model for the Prediction of Velocity and Void Fraction Profiles in Two-Phase Flow

F. C. BROWN and W. L. KRANICH

Worcester Polytechnic Institute, Worcester, Massachusetts

An experimental study of velocity and void-fraction profiles has been carried out for the cocurrent two-phase flow of both air and water, and air and glycerine-water systems. The investigation was restricted to flow in a horizontal, 1 in. diam. tube with primary emphasis on the bubble flow regime. The assumptions which must be made to reduce the general equations of continuity, momentum, and energy to the forms appropriate for two-phase flow are presented and the equations simplified for the case of no local slip. A model is proposed which allows the determination, by trial, of the two-phase velocity and void-fraction profiles. The profiles generated by the use of the model in conjunction with experimental sampling data are presented, the profile shapes are discussed, and their variations with Reynolds and Froude numbers and gas volumetric flow fraction are shown to be self-consistent. The horizontal profiles are found to be in fair agreement with those predicted from Levy's mixing length theory. A correlation scheme is outlined which, supplemented by data over wider ranges of operating conditions, would serve as a method for estimating pressure drops in two-phase flow.

Until recently most experimental investigations of two-phase flow consisted simply of the measurement of the total pressure drop and volumetric average void fraction, and were directed towards the establishment of general correlations. Typically, if the correlation schemes attempted to embrace all flow conditions, as Martinelli's (*21*), the uncertainties would be rather large. If attempts were made to specify phase distributions, as in homogeneous (*12*) or separated (*7*) flow, the results would be restricted to rather narrow ranges of operating conditions.

Only recently has more information on the fundamental nature of two-phase flow become available. Although limited to the determination of chordal averages, the development of X- or γ-Ray penetration techniques resulted in a more detailed knowledge of the variation of local void fraction with operating conditions (*16*). Neal (*23*) has developed a conductivity probe which permits the direct measurement of local void fraction, as well as bubble size and frequency distributions, for the two-phase flow of a gas and a nonwetting fluid. Nassos and Bankoff (*22*) have extended probe applications to aqueous systems.

If a two-phase stream could be sampled isokinetically, the true local void fraction, as well as velocity, would be obtained. Adorini and coworkers (*1, 2*) have developed sampling probes, in which stream static pressures are matched to a corrected probe inlet pressure, which withdraw samples of the two-phase mixture isokinetically. The difficulties involved in making the correction for friction losses in the probe entrance limit the usefulness of this technique. A Pitot tube cannot be used to determine two-phase velocities unless the behavior of the stream in the vicinity of the tube tip is specified. Attempts to do this, both analytically and experimentally, usually meet with only limited success as may be seen, for example, in the systematic nature of the deviations in the material balances presented by Gill (*13*).

Two-phase flow models based on simplified geometric descriptions of phase velocity and void fraction distributions have been shown repeatedly to be inadequate. The greatly simplified momentum and energy equations derived for these special cases cannot represent the flow situation as it actually exists. Recently, more realistic approaches have been taken in the derivation of the equations appropriate for two-phase flow. Vohr (*26*) derived the mechanical energy equation for separated flow by weighting the individual phase equations by their contribution to the total flow, neglecting surface energy changes and frictional losses. Lamb (*18*) added the respective momentum and energy equations directly and made use of the parity of interfacial shear to simplify the combination. VanDeemter (*25*) presented the differential equations of continuity, momentum, and energy for dispersed two-phase flow. The dependence of velocity and void fraction on position must be known to evaluate these equations.

Aside from the difficulties involved in measurement, the facts that the profiles are nonsymmetrical, sensitive to small changes in operating conditions, strongly dependent on entrance and exit effects, and continually developing render the determination of the local area–averaged void fraction and momentum fluxes most difficult. Yet all this information is essential if the nature of the relation between the local momentum flux and wall shear stress, that is, the functional dependence of the two-phase friction factor on flow parameters, is to be accurately determined. Then the relative contributions of frictional, interfacial, elevational, and accelerational losses to the total pressure drop may be specified.

Rose (*24*) has developed a simple device for the direct measurement of the total local momentum flux so that, by adjusting operating conditions, its variation with flow parameters may be studied. Cravarolo (*8*) has also succeeded in measuring wall shear stress directly. Experimental difficulties, however, restrict the application of both techniques to the study of relatively steady, nonpulsing vertical flow.

THEORETICAL ANALYSIS

The key to the solution of problems in two-phase flow is the correct formulation of the equations describing the dynamics of the system with supplementation, when required, by a physically justifiable model. The general equations of continuity, momentum, and energy for two-phase flow may be formulated in a manner exactly analogous to that for the well known case of compressible single-phase flow. Since two phases are flowing, however, the mass velocity of each phase must be written as $\rho_\psi \alpha_\psi v_\psi$ since, while phase velocities are considered continuous, the presence of a phase at a given point in the flow field may be discontinuous. In addition, there are forces and energies that are peculiar to multiphase flow and must be considered when formulating the momentum and energy equations, namely interfacial shear, magnus spin forces,

and surface energies. The derivations must also treat effects due to fluctuations in the local values of pressure, velocity, density, void fraction, energies, and dissipation rates; local slip between the phases; nonuniform and nonsymmetric phase and velocity distributions; and radial and angular, as well as axial, flow. Such a derivation is presented elsewhere (*6*).

In general form these complex equations cannot be applied to the analysis of two-phase flow with existing data. Many simplifications and assumptions must be made before useful working relationships are obtained.

In the remainder of this section the authors' assumptions are rather completely stated in order that the limitations of their final equations may be clearly understood. While the final equations are formally similar to single-phase relationships, it should not be inferred that they are derived by analogy or that a homogeneous model is assumed.

The standard time–smoothing procedure is used to separate the steady from the fluctuating terms to permit evaluation of the effects of the latter. While velocity, void fraction, energies and rates of energy dissipation are assumed to be functions of r, θ and z, for the final steps in the derivations, the static pressure is assumed to be a function of z only, and the assumptions of adiabatic flow with no shaft work for flow in a conduit of a constant diameter are applied.

With currently available instrumentation, it is impossible to directly measure some of the functions occurring in the equations. Where approximations to these functions cannot be made, order of magnitude estimates of their effects are carried out in order to justify their retention or exclusion from final consideration.

The general differential equations of continuity, momentum, and energy are virtually impossible to evaluate. Considerable simplification results from integration over the direction normal to the bulk flow since normal velocities vanish, and surface energies vanish if the flow is single-phase in nature at the wall. One then simply evaluates the steady state equations at stations located a distance, ΔL, apart with the appropriate averaging with length performed where required.

In the momentum equation, no distinction has been retained between any components of force due to interfacial shear, surface tension, or magnus spin forces and the shear stress due to turbulent transport along velocity gradients. The resulting simplified shear stress need not be linear in r, symmetric in θ, or zero at the centerline of the conduit.

In the energy equation, it was assumed that there is no mass transfer between the phases. In general, the local rate of irreversible energy dissipation in two-phase flow may include loss mechanisms other than viscous dissipation which are characteristic of two-phase flow. However, if all potential mechanisms are considered, it is possible to show by using simplified models and order of magnitude assumptions that essentially all of the energy irreversibly dissipated is lost at the wall (*6*). It may also be shown that unless bubble sizes are extremely small, mass flow rates low, or agglomeration severe, changes in surface energy with length are negligible.

The resulting much simplified equations are still more complex than the corresponding single-phase forms in that the phases still may have different local velocities and densities and the groupings involving products and sums of fluctuating terms cannot be eliminated a priori. This results from the fact that the structure of the two-phase stream is constantly developing along the path of flow. Thus, even though a long entrance or calming section may be used, two-phase flow is never fully developed in the single phase sense. Although there is no method currently available to directly measure either the absolute magnitude or the change in magnitude with length of these terms, they may be expected to be small with respect to the other terms in the equations, by analogy to the development of single-phase flow.

For gas-liquid, two-phase flow at low pressures, in which $\rho_l >> \rho_g$ and $\mu_l >> \mu_g$, the assumption of no local axial slip is most closely met in the bubble flow regime. In this regime, the liquid phase is continuous and, particularly in horizontal flow, the individual gas bubbles move axially with the more dense, viscous liquid phase at a velocity very nearly equal to that of the continuous phase. In order to allow for redistribution of the phases, however, some true local slip must be permitted in the r and θ directions.

The continuity, momentum, and energy equations for two-phase flow in the bubble flow regime, then, are reduced to the form:

Continuity;

$$\Delta(\overline{\rho_{TP}v_{TP}}^{R\theta}) = 0 \tag{1}$$

Momentum;

$$-\Delta p_{TP} = \frac{2\Delta L}{R}\overline{\tau_{RZ}}^{L\theta} + \Delta(\overline{\rho_{TP}v^2_{TP}}^{R\theta}/g_c) - \frac{g}{g_c}\cos\phi\Delta\overline{L\rho_{TP}}^{RL\theta} \tag{2}$$

Energy;

$$-\frac{1}{2g_c}\Delta(\overline{v^3_{TP}}^{R\theta}/\overline{v_{TP}}^{R\theta}) - \frac{g}{g_c}\cos\phi\Delta L - \int_{p_{L_o}}^{p_{L_o}+\Delta L}(1/\overline{\rho_{TP}}^{R\theta})\,dp_{TP} = \overline{H_{fTP}}^{L\theta} \tag{3}$$

These equations are basically of the same form as those derived by Lamb and White (*17*) using a somewhat different approach. It should be emphasized, however, that they do not represent what is called *homogeneous flow* since they require integration of nonuniform phase distributions over the flow path. They do reduce to the homogeneous form if the profiles are uniform, but the assumptions of no local slip and uniform phase distributions are probably mutually exclusive.

As has been pointed out, the direct determination of the local values of velocity, void fraction, and wall shear stress needed to evaluate these equations is quite difficult. When a local sampling technique is used, the measured value of local void fraction is a function of the rate at which the sample is withdrawn. To overcome these problems a procedure is required which determines the local velocity-void fraction relationship, specifies the resulting velocity and void fraction profiles, and permits the calculation of average local wall shear stress from a knowledge of the locally existing flow conditions. Experimental studies showed that if, in the bubble flow regime, measured Pitot tube impact pressures and sampling data were interpreted in such a manner that the integrated profiles were forced to satisfy the continuity equation, the resulting velocity position data would fall about the well known universal velocity profile curve for single-phase flow (*6*). The lack of exact agreement could be ascribed to the rather crude method of necessity used to interpret the Pitot tube data.

It may also be noted that, for the case of two-phase flow in which the simplifying assumptions which lead to Equations (1), (2), and (3) are justified, the equations of continuity, momentum, and energy and the expression of the universal velocity profile are all formally similar to the same single-phase relationships. At the same time, the flow itself may be quite two phased in nature, and strongly un-

symmetrical in gas distribution.

Hence, for two-phase flow with no local axial slip, no mass transfer between the phases, negligible fluctuating and surface energy terms, a wetting liquid, and moderate pressure drops, it is proposed that the two-phase velocity profile is formally similar to the corresponding single-phase profile. As a corollary, it is proposed that it is possible to predict the local average wall shear stress in a manner formally similar to that used in single-phase flow. All that is needed is experimental sampling data to specify the local sampling velocity-void fraction relationship and it becomes possible to compare the results predicted by use of this model with experimentally determined values of pressure drop and volumetric average void fraction by proper evaluation of the terms in Equations (1), (2), and (3).

The velocity profile with which formal similarity is assumed is the logarithmic distribution law form of the dimensionless velocity and position variables suggested by Prandtl with the empirical constants determined from the data of Deissler (9). These particular dimensionless forms for expressing velocity-position data have been used with some success, in two-phase flow, to describe profiles in the liquid film in vertical annular flow (19) and in the gas phase when flow is completely separated (14). Levy's mixing length theory generates a plot of this profile with the dimensionless centerline void fraction as a parameter (20). When formally similar two-phase functions are introduced, the universal velocity profile may be written:

$$v_{TP}(\rho_{TP}/\overline{\tau}^{\theta}_{RZ}g_c)^{1/2} = K_1 \ln[(R-r)(\overline{\tau}^{\theta}_{RZ}g_c/\rho_{TP})^{1/2}\rho_{TP}/\mu_{TP}] + K_2 \quad (4)$$

Thus, if $\overline{\tau}^{\theta}_{RZ}$ is specified, the local relationship between velocity and void fraction (the general form of which may be obtained from sampling experiments) which is necessary to satisfy this equation is fixed. There remains the task of calculating $\overline{\tau}^{\theta}_{RZ}$ from a knowledge of the locally existing flow conditions.

The wall shear stress in single-phase flow may be calculated from the well known Fanning relation, $\tau_{RZ} = \frac{f}{2}\rho V^2/g_c$. That is, the wall shear stress is proportional to the momentum flux, and the proportionality constant, the friction factor, is a function of the ratio of the momentum forces to the viscous forces through the Reynolds number. Among the assumptions which were made leading to the development of Equations (1), (2) and (3) were those which implied that there was no distinction between turbulent and interfacial shear stresses. They minimized the contribution of mechanisms peculiar to two-phase flow to the total rate of irreversible energy dissipation. This equals the assumption that, as in single-phase flow, the wall shear stress is proportional to the momentum flux and that if the mechanisms are the same, the proportionality constant, (that is, the friction factor) must be the same. Since the two-phase momentum flux is not $\rho\overline{(v)}^{R\theta 2}/g_c$ but $\overline{(\rho v^2)}^{R\theta}/g_c$, it is necessary to redefine the proportionality constant as:

$$\tfrac{1}{2}f = \frac{\overline{\tau}^{\theta}_{RZ}g_c}{\rho\overline{v^2}^{R\theta}} \quad (5)$$

The relationship between f and f may be obtained from single phase profiles (with ρ not varying with radius), and is the well known momentum correction term $\overline{v^2}^{R\theta}/\overline{(v)}^{R\theta 2}$. It also follows that the proportionality constant must be a unique function of a Reynolds number, but the Reynolds number as usually defined, $N_{Re} = DV\rho/\mu = \rho(V)^2/(\mu V/D)$, does not represent the ratio of local momentum to viscous forces in two-phase flow. A more appropriate definition in this case is

$$N_{Re} = \overline{\rho v^2}^{R\theta}/(\overline{\mu v/D}^{R\theta}) \quad (6)$$

Again, N_{Re} is related to N_{Re} through the momentum correction term. One consequence of this definition, however, is that unless over a finite path of flow, $\dot{Q}_{TP}/\dot{Q}_{TP} = \Delta\overline{\rho v^2}^{R\theta}/\Delta\overline{\rho v^2}^{R\theta}$, the value of N_{Re} will be a function of length.

The appropriate relationship between f and N_{Re} for use in calculations for smooth tubes is

$$f = 0.00144 + 0.138(N_{Re})^{-0.331} \quad (7)$$

It should be emphasized that these relations are valid only over the restricted range in which the assumptions leading to Equations (1) to (3) are valid. For instance, where significant interfacial shear exists, the wall shear will not be proportional to the total momentum flux alone. It is not the purpose of this model to treat these more complex, although more numerous, cases.

At this point the only function in the preceding set of equations which has not been defined is μ_{TP}, the viscosity appropriate for use in two-phase flow in this model. Analysis of the experimental velocity profiles in single-phase flow shows that the molecular viscosity is important with respect to the so called "eddy viscosity" only very close to the wall of the conduit. In the formulation of Prandtl's profile, the characteristic viscosity is unambiguously taken as the molecular viscosity even though this has real physical significance only very close to the wall. This device eliminates the need to define a viscosity which is a function of the structure of the field of flow. In the bubble flow regime, where the liquid completely wets the wall and there is little penetration of the gas phase into the liquid layer adjacent to the wall, the two-phase viscosity is nearly equal to the liquid viscosity. (The exact value would be a function both of local void fraction and the geometry of the phase distributions.) The most characteristic viscosity for use in this model, then, is the liquid viscosity.

The preceding equations and definitions are sufficient for the solution, by trial and error, of the dimensionless velocity profile for both velocity and void fraction distributions according to the following procedure:

1. Traverse the tube, withdrawing the two-phase mixture at various rates, to establish the local relationships between sampled velocity and sampled void fraction. Somewhere within the velocity range investigated at every location the sampling will have been truly isokinetic (although initially this particular velocity is unknown).

2. Assume a value for $\overline{\tau}^{\theta}_{RZ}$

3. At each location sampled, find the values of v_{TP} and α_ψ which simultaneously satisfy the relationship established in 1 and the universal velocity profile Equation (4).

4. Integrate the profiles thus generated to obtain values of $\overline{\rho_{TP}v^2_{TP}}^{R\theta}$ and $\overline{v_{TP}}^{R\theta}$. With these functions N_{Re} may be calculated and the corresponding value of f obtained from Equation (7). The value of $\overline{\tau}^{\theta}_{RZ}$ consistent with the profiles obtained in 3 may then be caculated from Equation (5).

5. Compare the calculated and assumed values of $\overline{\tau}^{\theta}_{RZ}$.

If they are not equal, a better guess is made for $\overline{\tau}^{\theta}_{RZ}$ and the procedure is repeated from 3 onward.

6. When the assumed and calculated values of $\overline{\tau}^{\theta}_{RZ}$ are the same, the profile is entirely self-consistent and, if the modeling is correct, the sampling has been isokinetic everywhere.

At any location along the path of flow the results generated by this model may be checked against the metered volumetric flow rates since velocity-void fraction–position data were generated and

$$\dot{Q}_{TP} = \dot{Q}_L + \dot{Q}_G = \int_o^{2\pi} \int_o^R v_{TP} r dr d\theta$$

and

$$\dot{Q}_\psi = \int_o^{2\pi} \int_o^R v_{TP} \alpha_\psi r dr d\theta$$

Results evaluated at stations ΔL apart would allow evaluation of the continuity, momentum, and energy equations providing that the appropriate averaging in L could be performed. Over short lengths linear averages should suffice. The volumetric average void fraction may be obtained by a simple trapping experiment and compared with that calculated from the model by properly integrating the local void fractions. The FORTRAN listing of programs for the computation of these procedures is presented elsewhere (6).

It should be emphasized that the integration of the profiles which generates data necessary to check the continuity equation tends to mask errors in the details of the profiles. Agreement with continuity and volumetric average void fractions is a necessary but not sufficient condition for establishing the validity of the generated profiles. In addition, they must be physically reasonable and in agreement with qualitative and quantitative observations previously made.

EQUIPMENT AND PROCEDURE

The equipment used in this investigation, shown schematically in Figure 1, was constructed to allow control and metering of the flow rates of each phase, control of the static pressure in the test section, and measurement of the total pressure drop, pressure fluctuations, and average void fraction in the test section. Probes were developed which permitted measurement of the local values of velocity, void fraction, and impact pressures within the test section.

The test section was a 10 ft. length of 1 in. nominal I.D. glass pipe. A sampling section, used as a mount for the Pitot and sampling tubes and as a pressure measuring station, was located downstream from the test section.

Measurement of the amount of liquid in the test section under operating conditions was obtained by simultaneously closing ball valves located at either extreme of the test section and draining and measuring the trapped liquid. A gate valve, positioned horizontally and located at the entrance to the disengaging tank, was used to adjust the static pressure in the test section during a run.

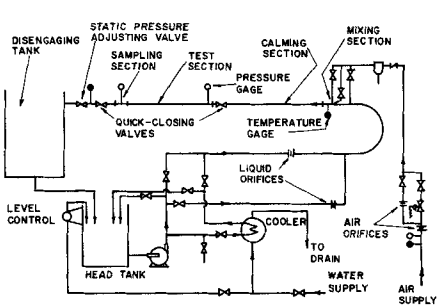

Fig. 1. Schematic diagram of the test set up.

The horizontal and vertical sampling tubes were designed to permit true isokinetic sampling in two-phase flow. A large tube size, ⅛ in., was chosen so that during sampling at the highest flow rates, the static pressure of the system would still be a sufficient driving force to overcome the frictional losses in the sampling train. A 1/32 in. diam., 3/8 in. long knife-edge extension was added to reduce the mass flow rate of fluid required for a given velocity and to eliminate liquid spillover resulting from the inability of the liquid phase to be accelerated around a blunt tip. The flow rate through the sampling tube was controlled by clamping a flexible Tygon tube which transported the sampled two-phase mixture from the tube to the measuring system.

At the start of a run series, the air and liquid flow rates required to give the desired flow conditions were selected. After the initial transients had died out, the manometer leads were opened and final adjustments were made in the flow rates of each phase and the system static pressure. A sampling tube was then positioned at the desired location and the local two-phase mixture withdrawn at four different flow rates. The rates were chosen so as to have two sampling velocities higher and two lower than the anticipated true local velocity and a total variation in sampled velocity of at least a factor of two.

Upon completion of the local sampling series, the appropriate Pitot tube was positioned and, after the impact pressure ceased to change, the reading was recorded. The Pitot tube was then withdrawn flush with the wall and the sampling tube repositioned.

Sampling of the stream was carried out at the centerline and at distances of 0.400, 0.300, 0.200, 0.130, and 0.063 in. from the wall. Half the diameter was traversed horizontally and symmetry was assumed, but the vertical traverse of the complete diameter was taken. Representative values of temperature, pressure, orifice pressure differences, and total pressure drop were also recorded.

The local sampling data, together with the sampling tube tip area, atmospheric, and local static pressure were used as inputs to a series of computer programs. Following the procedure previously outlined, the programs first converted the local sampling rates to local velocity-void fraction data and curve fitted by a least squares technique, the results at each sampling location to a relation of the form $\alpha_\psi = K_1 + K_2 v_{TP} + K_3 v^2_{TP}$. To reduce the number of iterations, the experimental value of $\overline{v_{TP}}^{R\theta}$ and an estimate of $\overline{\rho_{TP} v^2_{TP}}^{R\theta}$ were used instead of $\overline{\tau}^{\theta}_{RZ}$ to start the trial and error procedure of fitting the local sampling data to the universal velocity profile.

With the curve fitted local data, physical properties data, and the average velocity and momentum flux estimate as input, the main program calculated a set of local velocity–void fraction data which were consistent with the Deissler profile and the modified Fanning relation.

These calculated data were then used as input to a third program which integrated the profiles to give calculated values of $\dot{Q}_{TP}$, $\dot{Q}_G$, $\overline{\alpha_G}^{R\theta}$ and $\overline{\tau}^{\theta}_{RZ}$. The calculated and experimental volumetric flow rates could be compared directly.

The conditions for the next run series were then selected so that the mass and volumetric flow rates obtained at the upstream end of the test section for the previous series were obtained at the downstream location for the new series. The procedures described in the preceding paragraphs were repeated and a new set of data was generated to calculate $\dot{Q}_{TP}$ $\dot{Q}_G$ $\overline{\alpha_G}^{R\theta}$, and $\overline{\tau}^{\theta}_{RZ}$. The two series together closely simulated conditions upstream and downstream of the test section for a single set of gas and liquid mass flow rates. With these data for stations at the extremes of the test section, sufficient information had become available to solve the momentum and energy equations for the test section. In this manner the calculated pressure drop, head loss, and volumetric averaged void fraction could be compared with the experimentally determined values to test the validity of the model.

As a check on the program and method, single-phase data were used and the average deviations between calculated and experimental results were found to be 0.6% in volumetric flow rate and 3.1% in pressure drop over the range of liquid flow rates investigated.

The equipment used in this study provided for the use of three different types of gas injection configurations. In order to determine whether an entrance effect would persist after the two-phase mixture had passed through a calming section 170 diam. in length, a series of runs was made in which only the method of mixing the phases was varied. While a definite entrance effect was noted for annular mist flow, the average deviation between maximum and minimum pressure drop for the different injection arrangements for bubble flow was only 0.6%. It may be concluded, therefore that there are no entrance effects associated with the results presented herein.

PROFILES

Some typical two-phase velocity and void fraction profiles generated by the use of this model and experimental sampling data are shown in Figures 2 to 4. The velocity and void fraction profiles for a given run are not independent since V^+ is a function of both v_{TP} and ρ_{TP}, and S^+ is a function of ρ_{TP} for a given $\frac{\theta}{\tau_{RZ}}$. Therefore, alteration of the void fraction profile, that is, the redistribution of the phases, must be accompanied by a corresponding change in the velocity profile. Thus, although the dimensionless velocity profile is symmetric, the actual velocity and void fraction profiles are not.

An analysis of the causes for the development and subsequent modification of the phase distribution reduces, essentially, to a consideration of the forces which cause phase segregation. If phase densities are fixed, the gravitational force is invariant and, if other physical properties do not change, the surface tension and molecular viscosity forces are also invariant. All other forces, spin forces and effects dependent on eddy viscosity for example, are functions of the field of flow.

It is to be expected, therefore, that the dimensionless ratios which represent the ratio of momentum to viscous forces, momentum to gravitational forces, and momentum to surface forces (the Reynolds, Froude, and Weber numbers respectively) should characterize two-phase velocity and void fraction profiles.

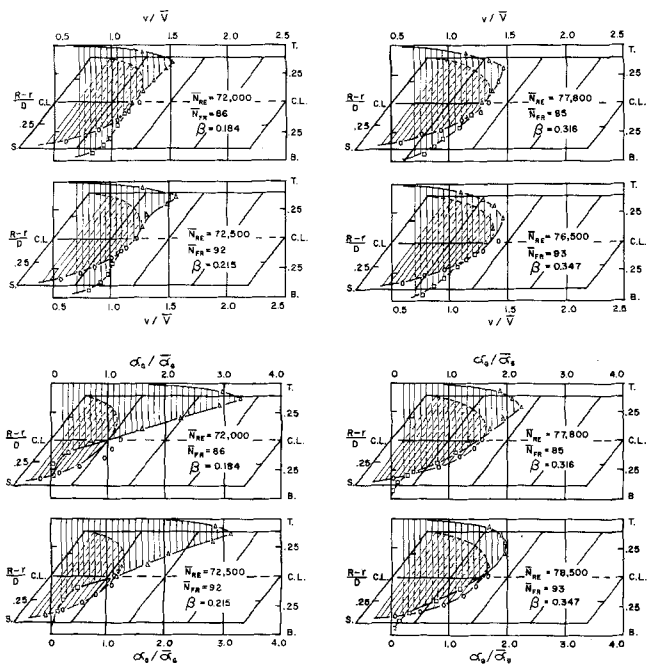

Fig. 2a, b, c, d. Effect of variation of gas volumetric flow fraction on velocity and void fraction profiles at constant Reynolds and Froude numbers.

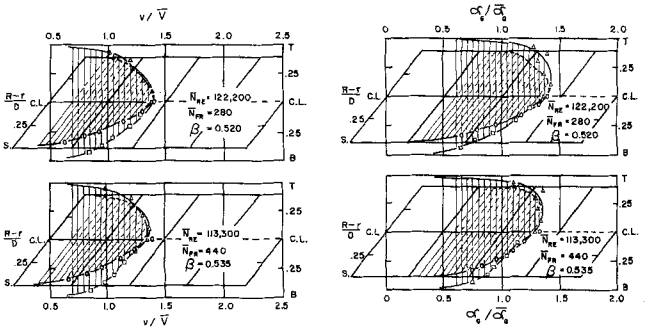

Fig. 3a, b. Effect of variation of Froude number on velocity and void fraction profiles at constant Reynolds number and gas volumetric flow fraction.

In addition, the profile shapes will be a function of the local area-average volumetric flow rate ratio, β, which is a measure of the extent of deviation from a single-phase condition. Since interfacial tension was not a controlled variable in these experiments, the Weber number is not treated as a characterizing parameter here.

The most striking characteristics of the two-phase profiles in horizontal flow are quite evident; compared with single-phase profiles they are steep and asymmetric.

If the Reynolds and Froude numbers are held constant and β is increased, the ratio $\alpha_{G\max}/\overline{\alpha_G}^{R\theta}$ decreases sharply as shown in Figure 2. Both Reynolds and Froude numbers here are defined using the integrated momentum flux. As the volume fraction of gas increases, the gas crowds its way out of the upper quadrant and more uniformly occupies the area of the pipe. At a given set of Reynolds and Froude numbers, there will be a critical value of β beyond which this generalization will no longer be valid because of a transition from the bubble to the annular, slug, plug, or stratified flow regimes depending on the total mass and volumetric flow rates. The complete definition of these transitions would constitute a regime map.

If the Reynolds number and β are fixed and the Froude number is increased, the ratio $\alpha_{G\max}/\overline{\alpha_G}^{R\theta}$ again decreases as shown in Figure 3. The effect is especially noticeable at low values of $\mathbf{N}_{Fr}$ and β where the profiles are quite steep and even a moderate increase in the ratio of momentum to gravitational forces is sufficient to distribute the gas phase much more evenly. The reduction of this ratio as the Froude number tended towards infinity, as for zero g, would eventually cease, as the surface forces (the spin forces) would still operate in the absence of body forces.

Finally, if the Froude number and β are fixed and the Reynolds number is increased, the ratio $\alpha_{G\max}/\overline{\alpha_G}^{R\theta}$ again decreases as shown in Figure 4. This effect is not nearly as pronounced as the $\beta|\mathbf{N}_{Re}$, $\mathbf{N}_{Fr}$ and $\mathbf{N}_{Fr}|\mathbf{N}_{Re,\beta}$ variations,

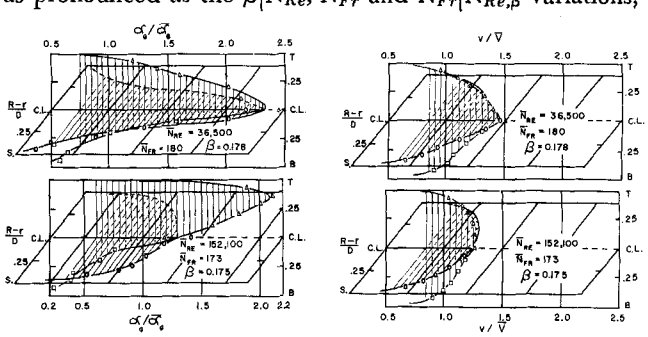

Fig. 4a, b. Effect of variation of Reynolds number on velocity and void fraction profiles at constant Froude number and gas volumetric flow fraction.

but it is again in the direction expected, since a lower shear rate, resulting from a lower viscosity, for a given momentum flux will tend to decrease the spin forces which prevent uniform distribution.

The profile data from twenty-nine runs were fitted, by a least squares technique, to a power law relation to obtain the functional dependence of the ratio of maximum to average void fraction on Reynolds and Froude numbers and gas volumetric flow fraction. The following equation was obtained:

$$\alpha_{G\max}/\overline{\alpha_G}^{R\theta} = 2{,}250(N_{Re})^{-0.082}(N_{Fr})^{-0.25}(\beta)^{-0.20} \quad (8)$$

The average deviation between calculated and experimental ratios is 9.7%, but the values of the exponents may well be subject to change outside of the range of variables investigated; $20{,}000 < N_{Re} < 175{,}000$, $50 < N_{Fr} < 700$, $0.10 < \beta < 0.60$.

The two-phase velocity profiles reflect the effect of N_{Re} at constant N_{Fr} and β in the same manner as do the void fraction profiles, the ratio $v_{\max}/\overline{v_{TP}}^{R\theta}$ decreasing as N_{Re} increases. This behavior is entirely analogous to single-phase flow. With Reynolds number and β held constant the profiles become flatter, $v_{\max}/\overline{v_{TP}}^{R\theta}$ decreasing, with increasing Froude number. This effect is small, reflecting chiefly the redistribution of phases brought about by the increase in the momentum forces.

Lastly, with Reynolds and Froude numbers fixed the ratio of maximum to average velocity decreases as β decreases. This phenomenon, occurring simultaneously with the marked increase in $\alpha_{G\max}/\overline{\alpha_G}^{R\theta}$ reflects the approach of the two-phase velocity profiles to the familiar, relatively flat, single-phase forms as β goes to zero. It is to be expected that beyond some critical value of β the variation would be in the opposite sense, the profiles becoming flatter as β tended towards unity, the other single-phase condition.

In general, the variations in the velocity profiles are much less severe than those of the void fraction profiles in the bubble flow regime. This is evident both from Figures 2 to 4 and the magnitude of the exponents on the power-law least-squares fit of the velocity profile–Reynolds number–Froude number–β data which results in the following equation:

$$v_{\max}/\overline{v_{TP}}^{R\theta} = 500(N_{Re})^{-0.076}(N_{Fr})^{-0.062}(\beta)^{0.076} \quad (9)$$

The average deviation between calculated and experimental ratios for this equation is 3.8%.

All of the velocity profiles have certain characteristics in common. Their flatness in relation to the void fraction profiles is obvious. All have their point of maximum velocity displaced above the center of the pipe and, consequently, do not necessarily have a point of zero shear on the centerline. The mixtures support a higher shear rate for a given shear stress in the upper quadrant because the increased concentration of the gas phase, with its low viscosity, reduces the effective stress-rate proportionality constant, the two-phase viscosity.

Another unusual feature is the occurrence of definite local maxima and minima in the slopes of the velocity curves. These changes of slope clearly reflect the changes in the distribution of the gas phase. This point may be illustrated by considering a simplified model for separated flow with no interfacial shear in which the abrupt change in the velocity profile would be due to the abrupt change in fluid viscosity. While such changes occur more gradually in bubble flow, it was nonetheless possible, for runs with low values of N_{Fr} and β, to visually establish quite definite boundaries between regions of high and low gas concentration as may be seen in Figure 2. The void fraction profiles show that similar gradients exist at higher values of β but they are much more difficult to define visually.

The displacement of the points of maximum velocity and void fraction from the centerline and the undulating nature of the shapes render a simple, mathematical description of the profiles most difficult. Knowing the ratio of maximum to average velocity and void fractions, it is possible to assign an exponent to a power law fit of the profiles by using the conditions that the integrated profiles must equal the averages. But a power law fit clearly is not representative of the experimental profiles obtained although it may serve better for vertical flow.

Few other experimental data are available to check, in detail, the profiles calculated using this model. Adorini's data, for vertical upwards annular flow (*1, 2*), show profiles which are similar to those presented here, in that they are steeper than single-phase profiles. Armand's data, for horizontal flow in a 1 in. pipe, are expressed as the ratio of horizontal chordal average phase volumetric flow rates to the total phase volumetric flow rate. No attempts were made to obtain isokinetic sampling, but the profiles roughly indicate the changes in phase distribution with operating conditions. The trend, even to the local maxima in slope, is the same as indicated by the profiles of Figures 2 through 4 (*3*). The data of Nassos and Bankoff (*22*), although forced into a power law fit, actually show similar complex curvature in local α to that observed here.

The only theoretically based method currently available for the prediction of two-phase velocity and void fraction profiles is Levy's mixing length theory (*20*). The treatment is based directly on an analogy to single-phase flow and, as such, cannot predict the occurrence of either nonsymmetric profiles or local maxima or minima in the slopes of the profiles. It is inherently restricted to vertical flow in which no large discontinuities in phase distribution occur. However, for purposes of comparison the horizontal profiles of certain experimental runs were contrasted with the shapes predicted by Levy's theory for the corresponding operating conditions. The average deviation between experimental and calculated values for six run conditions was 5.4% in velocity and 0.047 in void fraction. In the bubble flow regime Levy's profiles are biased, almost all predicted velocities are too low, and are noticeably flatter than the experimental ones. As the character of the flow shifted towards slug flow the theoretical profiles became steeper than the experimental ones but the low bias remained. The calculated void fraction profiles are also flatter than the experimental ones, with experimental gas void fractions generally lower than predicted. Still, it must be admitted that there is no reason to believe that the horizontal profiles of a two-phase mixture flowing horizontally should be exactly the same as those for vertical flow. Thus, even though the results predicted by the mixing length model differ in detail from the experimental results, they are certainly of the correct order of magnitude.

It has been suggested (*10*), based on similarity considerations, that the viscosity appropriate for use in two-phase flow is a complex function of local liquid and gas viscosities, void fractions, velocities and velocity gradients. For the case of no-slip homogeneous flow the function is simplified and the resulting two-phase viscosity is written in the form, $\mu_{TP} = \mu_L\alpha_L + \mu_G\alpha_G$. The use of such a viscosity in the procedure presented herein results in either profiles which are significantly steeper than those shown in Figures 2 through 4 but which do not satisfy the continuity, momentum, and energy equations when integrated

or do not permit self consistent results to be obtained from the trial and error technique previously outlined (that is, the computer program diverges). Self-consistency is obtained when the significant viscosity is taken as that of the fluid immediately adjacent to the wall, (that is, the liquid viscosity) as discussed earlier in this paper.

PROFILE INTEGRATION

If the proposed model for characterizing two-phase flow profiles is correct, the integrated profiles must satisfy the continuity equations, and, with the modified Fanning equation, the momentum and energy equations must predict the correct pressure drop and head loss respectively. Also, the void fraction profile must integrate to give the correct volume-average void fraction.

The assumptions leading to the simplification of the general equations to the forms of Equations (1), (2), and (3), particularly the assumption of no local axial slip, should be most closely met in the bubble flow regime. For values of gas volumetric flow fraction less than about 0.6 and two-phase Froude number greater than about 50, (approximately the limits for the transition to slug flow), the integrated two-phase velocity profiles agreed extremely well with the measured volumetric flow rates. The average absolute deviation in total volumetric flow rates for twenty-nine runs was 1.2% with a mean deviation of +0.5%. This may be considered an exact agreement within experimental error. While either the gas or liquid $v_{TP}\alpha_\psi$ profile may be integrated to give the corresponding phase volumetric flow rate, only one may be used as an independent check along with the total flow rate. The average absolute and mean deviations between calculated and experimental gas volumetric flow rates were 3.5 and +1.1% respectively, while those for the liquid were 3.0 and −0.8%. Although individual deviations were as high as 9.9%, the average deviations are small enough to be acceptable.

The availability of integrated profiles at the equivalent of both extremes of the test section permits the calculation of the volumetric average void fraction and the evaluation of all terms in the momentum and energy equations. The average absolute and mean deviations between calculated and experimental volumetric void fractions for eighteen determinations were 0.023 and +0.003 respectively, which is quite good agreement. The signs of the deviations in the calculated volumetric average void fraction correspond to the deviations in the calculated phase volumetric flow rates; for runs with a positive deviation in $\dot{Q}_G$, the deviation in $\overline{\alpha_G}^{R\theta}$ is also positive and vice versa.

The average absolute deviations between calculated and experimental pressure drops and head losses were 8.8 and 6.9% while the mean deviations were +2.4 and +3.8% respectively. The error in the calculation of two-phase pressure drop and head loss reflects errors of technique and method to a greater degree than does the calculation of phase flow rates and void fraction. In the Reynolds number region of interest, the frictional pressure drop varies approximately as the flow rate to the 1.8 power, so it is to be expected that deviations in the continuity equation will be amplified in the momentum and energy equations. If improper θ integration, or some other source of error, results in the calculation of a momentum flux which is higher than the actual value, the computer program responds by increasing the trial value still further making this procedure a rather sensitive one. The contribution of the calculated two-phase density to the error induced by an incorrect momentum flux is illustrated by the fact that the larger negative deviations in pressure drop occur for those runs with the larger positive deviations in $\overline{\alpha_G}^{R\theta}$ and vice versa. This also explains the smaller errors in the calculation of the head loss, as a high pressure loss is offset by a ρ_{TP} which is also somewhat too high. In view of these difficulties, the observed deviations between calculated and measured pressure drops and head losses are acceptable.

Since the profiles generated are consistent with the continuity, momentum, and energy equations and the measured phase distributions, it may be concluded that the proposed model adequately represents two-phase flow in the bubble flow regime.

GENERAL CORRELATIONS

Since the velocity and void fraction profiles in horizontal two-phase flow are nonsymmetric, vary widely with operating conditions, have different functional dependences on N_{Re}, N_{Fr}, and β [see Equations (8) and (9)], and are sensitive to entrance effects, it is reasonable to expect that simplified correlation schemes will be valid only in restricted ranges. In general, only overall average values, such as β or Q/A, are known a priori and the most successful correlation is the one which best relates the integrated distributions to these known values.

In order to evaluate elevation pressure losses or convert head loss to pressure drop, information on the variation of area average void fraction with flow parameters must be available. If profile shapes are known in detail, this may be calculated directly (*28*). When these data are not available, the approach proposed by Armand (*4*), relating $\overline{\alpha}^{R\theta}$ to β by a single constant K, might be used. Various other investigators (*5, 15, 27*) have found slightly different values for K and also that K was itself a weak function of pressure, Reynolds and Froude numbers, and β.

The data obtained in the present experiments were fitted to a relation of this form to give a calculated value of $K = 0.866$ with an average deviation between calculated and experimental void fractions of 0.014 ($\overline{\Delta\alpha_G/\alpha_G} = 4.3\%$). While this is well within the range of experimental error, negative deviations consistently occurred when the value of N_{Fr} was less than 150. This is consistent with Hughmark's observations (*15*) and, based upon the relative magnitudes of the exponents in Equation (8), one would also expect a similar trend involving β.

Examination of the simplified momentum and energy Equations (2) and (3) shows that, if one can relate wall shear stress to momentum flux, less information on the details of the phase distribution is necessary to solve the momentum than the energy equation. This, then, is the logical starting point for pressure drop correlations in two-phase flow. To solve the momentum equation, the value of the integral of $\rho_{TP}v_{TP}^2$ (the two-phase momentum flux) is needed to calculate both wall shear stress (using Equation (5)) and acceleration pressure drop. Rose (*24*) was able to relate the total two-phase momentum flux to that calculated by assuming average velocities and void fractions with a separated flow model as a function of β. The data obtained in the present experiments are shown, expressed on the same basis, in Figure 5. Three-fourths of the points lie within ±5% of the best line through the data. Thus, given mass and volumetric flow rates and the relation between $\overline{\alpha_G}^{R\theta}$ and β, the momentum flux can be estimated and the momentum equation solved.

The correlation was tested against experimental results for the conditions upstream of the last run in each constant-mass-flow rate series. The average and mean deviations were 6.6 and +4.3% with a maximum deviation of 19.5%. The data of Johnson (*17*) and Fried (*11*) for both isothermal and nonisothermal flow were tested

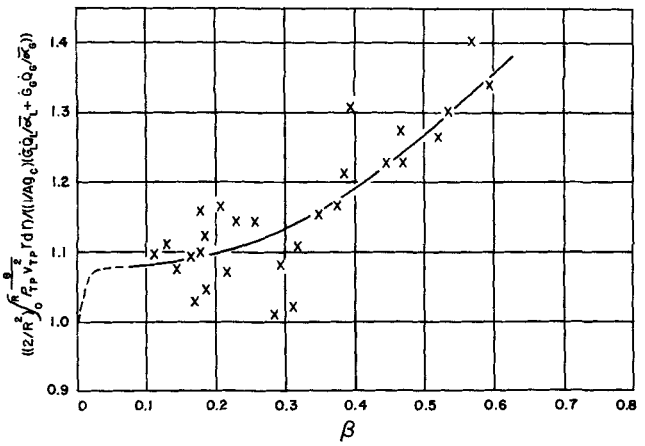

Fig. 5. Ratio of integrated momentum flux to that calculated from a separated flow model as a function of gas volumetric flow fraction.

against the proposed correlation and the average and mean deviations for fifteen runs were 9.1 and −7.6% with a maximum deviation of 21%. This agreement is as good as is usually found in two-phase flow correlations although the range of applicability is restricted to the bubble flow regime with $N_{Fr} > 50$ and $\beta < 0.6$.

As was the case with the constant relating $\overline{\alpha_G}^{R\theta}$ and β, the use of β alone as the independent variable results in deviations which are systematic. Positive deviations occurred for values of $N_{Re}/N_{Fr} < 850$ with negative deviations above this. Again, this is not surprising in light of the results of Equations (8) and (9). It seems likely that the correlation scheme could be improved by treating the ratio of Reynolds to Froude numbers, or the ratio $D^2 g \overline{\rho_{TP}}^{R\theta}/\overline{\mu v_{TP}}^{R\theta}$, as a parameter. This would require a regression analysis involving more data than are currently available.

CONCLUSIONS

For two-phase flow regimes in which it is appropriate to assume no local axial slip between the phases and negligible change with axial length of surface energy and fluctuating density, velocity, and void fraction terms, the continuity, momentum, and energy equations, integrated over the direction normal to the bulk flow, are formally similar to the well known single-phase equations. The requisite assumptions are met in the bubble flow regime.

A two-phase stream may be sampled isokinetically, with a properly designed instrument, and the sampling data fitted to the well known universal velocity profile.

The resulting velocity and void fraction profiles, which satisfy the continuity, momentum, and energy equations, are asymmetric and steeper than the corresponding single-phase profiles and show a continuous development with the path of flow. The profiles are in qualitative agreement with Levy's mixing length theory.

The measured momentum fluxes may be related to a momentum flux calculated from a separated model as a function, principally, of gas volumetric flow fraction. This is a logical starting point for the development of general correlations for the prediction of two-phase pressure drop.

ACKNOWLEDGMENT

The authors acknowledge the support of the Department of Health, Education, and Welfare through a Title IV grant to F. C. Brown during the course of this investigation.

NOTATION

A = pipe cross-sectional area, sq.ft.
D = pipe diameter, ft.
f = Fanning friction factor
f = friction factor defined in Equation (5)
G = mass velocity, $lb._m/sq.ft.\text{-}sec.$
g = gravitational acceleration, ft./sq.sec.
g_c = force-mass conversion factor, $ft.lb._m/lb._f sq.sec.$
H_f = frictional head loss, $ft.lb._f/lb._m$
K = a constant
L = length along the direction of bulk flow, ft.
N_{Fr} = Froude number, V^2/gD
N_{Fr} = Froude number, $\overline{\rho_{TP} v^2_{TP}}^{R\theta}/g\overline{D\rho_{TP}}^{R\theta}$
N_{Re} = Reynolds number, $DV\rho/\mu$
N_{Re} = Reynolds number defined in Equation (6)
p = static pressure, $lb._f/sq.ft.$
$\dot{Q}$ = volumetric flow rate, cu.ft./sec.
R = pipe radius, ft.
r = local radius, ft.
S^+ = dimensionless distance from wall, $(R - r)(\overline{\tau_{RZ}}^{\theta} g_c/\rho_{TP})^{1/2}\rho_{TP}/\mu_{TP}$
V^+ = dimensionless velocity, $v_{TP}(\rho_{TP}/\overline{\tau_{RZ}}^{\theta} g_c)^{1/2}$
v = local axial velocity, ft./sec.
V = average velocity, $V = \dot{Q}/\pi R^2$, ft./sec.
z = axial distance, ft.

Greek Letters

α = void fraction
β = gas volumetric flow fraction, $= \dot{Q}_g/\dot{Q}_{tp}$
Δ = difference between functions evaluated a finite distance apart
θ = angle about the axis, radians
μ = viscosity, $lb._m/ft.\text{-}sec.$
ρ = density, $lb._m/cu.ft.$
τ_{qz} = shear stress or z direction momentum flux due to a velocity gradient in the q direction, $lb._f/sq.ft.$
ϕ = inclination of the test section from the vertical, radians

Subscripts and Superscripts

B = bottom
θ = angular direction
$C.L.$ = evaluated at $r = 0$
G = gas phase
L = liquid phase
max = maximum value
ψ = phase (either gas or liquid)
R = evaluated at the pipe wall
r = radial direction
s = side of pipe at a horizontal plane through centerline
T = top
tp = two-phase
z = direction of bulk flow
$\overline{\ }$ = average quantity (superscript)
$\underline{q}$ = integrated average in the q direction(s) (for example, $\overline{A}^{rz}$ = A averaged over r and z)

LITERATURE CITED

1. Adorini, N., P. Alia, L. Cravarolo, A. Hassid, and E. Pedrocchi, *C.I.S.E.* Rept. R-89 (1963).
2. ———, I. Casagrande, L. Cravarolo, A. Hassid, and M. Silvestri, *ibid.*, R-35 (1961).
3. Armand, A. A., *A.E.R.E. Translation*, 828 (1959).
4. *Ibid.*, 4490 (1961).
5. Bankoff, S. G., *J. Heat Transfer*, 82, 265 (1960).
6. Brown, F. C., Ph.D. thesis, Worcester Polytech. Inst. (1966).

7. Calvert, S., and B. Williams, *AIChE J.*, **1**, 78 (1955).
8. Cravarolo, L., A. Giorgini, A. Hassid, and E. Pedrocchi, *C.I.S.E.* Rept. R-82 (1964).
9. Deissler, R. G., *Natl. Advisory Comm. Aeron. Tech. Note*, No. 2138 (1950).
10. Duckler, A. E., M. Wicks, and R. G. Cleveland, *AIChE J.*, **10**, 44 (1964).
11. Fried, L., *Chem. Eng. Progr. Symp. Ser. No. 9*, **50**, 47 (1954).
12. Foltz, H. S., and R. G. Murray, *ibid., No. 30*, **56**, 83 (1960).
13. Gill, L. E., G. F. Hewitt, and P. M. C. Lacey, *Chem. Eng. Sci.*, **19**, 665 (1964).
14. Hanratty, T. J., and J. M. Endgen, *AIChE J.*, **3**, 299 (1957).
15. Hughmark, G. A., *Chem. Eng. Progr.*, **58**, 62 (1962).
16. Isbin, H. S., H. A. Rodriguez, H. C. Larson, and B. D. Pattie, *AIChE J.*, **5**, 427 (1959).
17. Johnson, H. A., and A. H. Abou-Sabe, *Trans. Am. Soc. Mech. Eng.*, **74**, 977 (1952).
18. Lamb, D. E., and J. L. White, *AIChE J.*, **8**, 281 (1962).
19. Lee, J., *Chem. Eng. Sci.*, **20**, 533 (1965).
20. Levy, S., Paper presented at the fifth National Heat Transfer Conference (1962).
21. Marainelli, R. C., L. M. K. Boelter, T. H. M. Taylor, E. G. Thomsen, and E. H. Morrin, *Trans. Am. Soc. Mech. Eng.*, **66**, 139 (1944).
22. Nassos, G. P., and S. G. Bankoff, *Chem. Eng. Sci.*, **22**, 661 (1967).
23. Neal, L. B., and S. G. Bankoff, *AIChE J.*, **9**, 490 (1963).
24. Rose, S. C., and P. Griffith, Paper presented at the eighth National Heat Transfer Conference (Aug. 1965).
25. VanDeemter, J. J., and E. T. Van der Laan, *Appl. Sci. Res. Sec.*, **A10**, 102 (1961).
26. Vohr, J., *AIChE J.*, **8**, 280 (1962).
27. Zuber, N., *J. Heat Transfer*, **82**, 255 (1960).
28. ———, and J. A. Findlay, *ibid.*, **87**, 453 (1965).

Manuscript received August 2, 1967; revision received January 25, 1968; paper accepted April 3, 1968.

Analysis of Steady State Shearing and Stress Relaxation in the Maxwell Orthogonal Rheometer

R. BYRON BIRD, and EVERETTE K. HARRIS, JR.

University of Wisconsin, Madison, Wisconsin

A nonlinear, integral viscoelastic model is used to predict the stresses in the Maxwell orthogonal rheometer. The resulting expressions indicate that the instrument yields data on material functions not heretofore measured, and also show how the data may be analyzed to get the complex viscosity. Expressions are given for stress relaxation after cessation of shearing. Some experimental data are analyzed to give model parameters.

The Maxwell orthogonal rheometer (*1*) is an interesting rheological instrument, because the flow is nonviscometric. Recently an analysis was given (*2*) for the steady state operation of this device. Because it is based on a rheological model which is inadequate, the analysis does not account for possible deviations from linear viscoelasticity. The analysis is repeated here using a model which is felt to be more appropriate; and, in addition, expressions describing stress relaxation (*3*) are given. It is hoped that these analyses will help to call attention to the capabilities of the Maxwell orthogonal rheometer as a rheological tool.

THE RHEOLOGICAL MODEL

We use here an integral model of the form (*4*):

$$\tau = -\int_{-\infty}^{t} m(t-t', II(t'))\left[\left(1+\frac{\epsilon}{2}\right)\overline{\mathbf{\Gamma}}-\left(\frac{\epsilon}{2}\right)\mathbf{\Gamma}\right]dt' \quad (1)$$

Here $\overline{\mathbf{\Gamma}}$ and $\mathbf{\Gamma}$ are strain tensors defined, in cartesian coordinates, by

$$\overline{\Gamma_{ij}} = \Sigma_m(\partial x_i/\partial x'_m)(\partial x_j/\partial x'_m) - \delta_{ij} \quad (2)$$

$$\Gamma_{ij} = \delta_{ij} - \Sigma_m(\partial x'_m/\partial x_i)(\partial x'_m/\partial x_j) \quad (3)$$

in which x_i and x_i' are the position coordinates at times t (current time) and t' (past time) respectively. The memory function $m(t-t', II(t'))$ is taken to be

$$m(t-t', II(t')) = \sum_{p=1}^{\infty} \frac{\eta_p}{\lambda_{2p}^2} \frac{e^{-(t-t')/\lambda_{2p}}}{1+\frac{1}{2}\lambda_{1p}^2 II(t')} \quad (4)$$